Probing the very-high-energy γ-ray spectral curvature in the blazar PG 1553+113 with the MAGIC telescopes

J. Aleksić[1], S. Ansoldi[2], L. A. Antonelli[3], P. Antoranz[4], A. Babic[5], P. Bangale[6], J. A. Barrio[7], J. Becerra González[8,25,⋆], W. Bednarek[9], E. Bernardini[10], B. Biasuzzi[2], A. Biland[11], O. Blanch[1], S. Bonnefoy[7], G. Bonnoli[3], F. Borracci[6], T. Bretz[12,26], E. Carmona[13], A. Carosi[3], P. Colin[6], E. Colombo[8], J. L. Contreras[7], J. Cortina[1], S. Covino[3], P. Da Vela[4,⋆], F. Dazzi[6], A. De Angelis[2], G. De Caneva[10], B. De Lotto[2], E. de Oña Wilhelmi[14], C. Delgado Mendez[13], D. Dominis Prester[5], D. Dorner[12], M. Doro[15], S. Einecke[16], D. Eisenacher[12], D. Elsaesser[12], D. Fidalgo[7], M. V. Fonseca[7], L. Font[17], K. Frantzen[16], C. Fruck[6], D. Galindo[18], R. J. García López[8], M. Garczarczyk[10], D. Garrido Terrats[17], M. Gaug[17], N. Godinović[5], A. González Muñoz[1], S. R. Gozzini[10], D. Hadasch[14,27], Y. Hanabata[19], M. Hayashida[19], J. Herrera[8], D. Hildebrand[11], J. Hose[6], D. Hrupec[5], W. Idec[9], V. Kadenius[20], H. Kellermann[6], M. L. Knoetig[11], K. Kodani[19], Y. Konno[19], J. Krause[6], H. Kubo[19], J. Kushida[19], A. La Barbera[3], D. Lelas[5], N. Lewandowska[12], E. Lindfors[20,28], S. Lombardi[3], F. Longo[2], M. López[7], R. López-Coto[1], A. López-Oramas[1], E. Lorenz[6], I. Lozano[7], M. Makariev[21], K. Mallot[10], G. Maneva[21], K. Mannheim[12], L. Maraschi[3], B. Marcote[18], M. Mariotti[15], M. Martínez[1], D. Mazin[6], U. Menzel[6], J. M. Miranda[4], R. Mirzoyan[6], A. Moralejo[1], P. Munar-Adrover[18], D. Nakajima[19], V. Neustroev[20], A. Niedzwiecki[9], K. Nilsson[20,28], K. Nishijima[19], K. Noda[6], R. Orito[19], A. Overkemping[16], S. Paiano[15], M. Palatiello[2], D. Paneque[6], R. Paoletti[4], J. M. Paredes[18], X. Paredes-Fortuny[18], M. Persic[2,29], J. Poutanen[20], P. G. Prada Moroni[22], E. Prandini[11,30,⋆], I. Puljak[5], R. Reinthal[20], W. Rhode[16], M. Ribó[18], J. Rico[1], J. Rodriguez Garcia[6], S. Rügamer[12], T. Saito[19], K. Saito[19], K. Satalecka[7], V. Scalzotto[15], V. Scapin[7], C. Schultz[15], T. Schweizer[6], A. Sillanpää[20], J. Sitarek[1], I. Snidaric[5], D. Sobczynska[9], F. Spanier[12], A. Stamerra[3], T. Steinbring[12], J. Storz[12], M. Strzys[6], L. Takalo[20], H. Takami[19], F. Tavecchio[3], P. Temnikov[21], T. Terzić[5], D. Tescaro[8], M. Teshima[6], J. Thaele[16], O. Tibolla[12], D. F. Torres[23], T. Toyama[6], A. Treves[24], P. Vogler[11], M. Will[8], R. Zanin[18] (The MAGIC Collaboration), F. D'Ammando[31,⋆] (for the *Fermi*-LAT Collaboration), A. Lähteenmäki[32,33], M. Tornikoski[32], T. Hovatta[32,34], A.C.S. Readhead[32], W. Max-Moerbeck[34], J.L. Richards[35] (Affiliations can be found after the references)

Accepted - Received -; in original form -

Mon. Not. R. Astron. Soc. **000**, 1–10 (2014) Printed 12 August 2014 (MN LATEX style file v2.2)

ABSTRACT

PG 1553+113 is a very-high-energy (VHE, $E > 100$ GeV) γ-ray emitter classified as a BL Lac object. Its redshift is constrained by intergalactic absorption lines in the range $0.4 < z < 0.58$. The MAGIC telescopes have monitored the source's activity since 2005. In early 2012, PG 1553+113 was found in a high-state, and later, in April of the same year, the source reached the highest VHE flux state detected so far. Simultaneous observations carried out in X-rays during 2012 April show similar flaring behaviour. In contrast, the γ-ray flux at $E < 100$ GeV observed by *Fermi*-LAT is compatible with steady emission. In this paper, a detailed study of the flaring state is presented. The VHE spectrum shows clear curvature, being well fitted either by a power-law with an exponential cut-off or by a log-parabola. A simple power-law fit hypothesis for the observed shape of the PG 1553+113 VHE γ-ray spectrum is rejected with a high significance (fit probability P=2.6 $\times 10^{-6}$). For the first time a VHE spectral shape compatible with an exponential decay has been found in a distant blazar ($z > 0.2$). The observed curvature is compatible with the extragalactic background light (EBL) imprint predicted by the current generation of EBL models assuming a redshift $z \sim 0.4$. New constraints on the redshift were derived from the VHE spectrum. These constraints are compatible with previous limits and suggest that the source is most likely located around the optical lower limit, $z = 0.4$. Finally, we find that the synchrotron self-Compton (SSC) model gives a satisfactory description of the observed multi-wavelength spectral energy distribution during the flare.

Key words: gamma rays: observations, blazar, BL Lac: AGNs: individual (PG 1553+113)

1 INTRODUCTION

PG 1553+113 is a blazar found as part of the Palomar-Green Catalog of UV-excess Stellar Objects (Green, Schimdt & Liebert et al. 1986). Its J2000 coordinates are R.A. 15h55m43.0s, Dec. +11d11m24.4s (Beasley et al. 2002). It was classified as a BL Lac object due to its featureless optical spectrum (Miller & Green 1983) and significant optical variability (Miller et al. 1988). As occurs in most BL Lac objects, the featureless optical spectrum prevents a spectroscopic redshift measurement. However, several limits have been provided based on indirect measurements (e.g. Sbarufatti et al. 2005, 2006). The most recent redshift lower limit was estimated using the host galaxy as a standard candle: $z > 0.24$ and $z > 0.31$, for absolute R band magnitudes $M_R = -22.5$ and $M_R = -22.9$, respectively (Shaw et al. 2013). Previously, a more stringent redshift lower limit of $z > 0.4$ was set by Danforth et al. (2010) based on the detection of intervening Ly-α absorbers. This estimation will be used throughout the paper. Danforth et al. (2010) also set a redshift upper limit of $z < 0.58$ based on the non-detection of any Lyβ absorbers at $z > 0.4$.

The very-high-energy (VHE, $E > 100$ GeV) γ-ray emission from PG 1553+113 was discovered independently and almost simultaneously by H.E.S.S. (Aharonian et al. 2006a) and MAGIC (Albert et al. 2007a) in 2005. The integral flux recorded by MAGIC at the time of the discovery was $F = (10.0 \pm 0.2) \times 10^{-11}\mathrm{cm}^{-2}\mathrm{s}^{-1}$ above 120 GeV, and the differential energy spectrum was well described by a power-law with a spectral index $\Gamma \sim 4$, compatible with the detection by H.E.S.S. The source has been monitored with the MAGIC telescopes since 2005. The results from the 2005-2009 observation campaigns can be found in Aleksić et al. (2012a). Modest flux variability of a factor of ~2.6 on a yearly time-scale has been detected at E>150 GeV, with an integral flux lying in the range from 1.4 to $3.7 \times 10^{-11}\mathrm{cm}^{-2}\mathrm{s}^{-1}$. The observed energy spectra were well fitted by power laws with spectral indices in the range $\Gamma \sim 3.6 - 4.3$.

Extragalactic VHE γ-rays can be absorbed on the way to the Earth via electron-positron pair production when interacting with optical-UV background photons from the extragalactic background light (EBL, Stecker, DeJager & Salamon 1992). The EBL is composed of diffuse light emitted by stars and IR light reprocessed by dust, redshifted by the expansion of the Universe (Hauser & Dwek 2001). The uncertainty on its spectral energy distribution (SED) and evolution through the history of the Universe still ranges from 20% to 50% at wavelengths 0.4 and 40 microns, respectively. This uncertainty is mainly due to difficulties in direct measurements.

During the past few years several different approaches have been developed to model the EBL (e.g. Franceschini et al. 2008; Kneiske & Dole 2010; Finke et al. 2010; Domínguez et al. 2011; Gilmore et al. 2012; Scully, Malkan & Stecker 2014) and despite the different techniques adopted the resulting EBL models show an overall agreement, differing only marginally.

The γ-ray absorption depends significantly on the energy of the VHE photon, the redshift-dependent SED of the EBL and the distance to the source. The observed flux (F_{obs}) can be expressed as

$$F_{obs}(E) = F_{int}(E) \cdot e^{-\tau(E,z)}, \quad (1)$$

where F_{int} denotes the intrinsic flux emitted by the source and τ the EBL optical depth as a function of the energy and redshift.

The EBL imprint on the VHE γ-ray spectrum can be used to set upper limits on the redshift of the source. This is done by assuming a particular EBL model and a criterion on the intrinsic spectrum, such as a maximum hardness for the reconstructed intrinsic spectrum or the absence of a spectral break with a pile-up at VHE in the reconstructed spectrum.

Different authors have used this γ-ray attenuation technique

⋆ Corresponding authors: J. Becerra González, email: josefa.becerra@nasa.gov, P. Da Vela, email: davela@pi.infn.it, E. Prandini, email: elisa.prandini@unige.ch, F. D'Ammando, email: dammando@ira.inaf.it

for PG 1553+113, leading to the following limits: $z < 0.74$ (Aharonian et al. 2006b), $z < 0.42$ (Mazin & Goebel 2007), $z < 0.66$ (Prandini et al. 2010). Limits on the EBL absorption can be estimated independently from EBL models using the VHE spectrum and the redshift of the source under the assumption that the emission of the source can be properly described by a synchrotron self-Compton (SSC) model (Mankuzhiyil et al. 2010). This method has previously been used on PG 1553+113 to derive constraints on the γ-ray horizon (Domínguez et al. 2013).

PG 1553+113 was detected in the high-energy (HE, $E > 100$ MeV) γ-ray band by the Large Area Telescope (LAT) on board the *Fermi Gamma-ray Space Telescope* (Abdo et al. 2010). The energy spectrum can be well fitted by a power-law with spectral index $\Gamma = 1.67 \pm 0.02$ and $F(E > 100\,\mathrm{MeV}) = (5.7 \pm 0.2) \times 10^{-9} \mathrm{cm}^{-2} \mathrm{s}^{-1}$ and its variability index is 93.5 (Nolan et al. 2012). Since the variability index is > 41.6 the source is variable on a monthly time-scale at >99% confidence probability. No flaring activity has been claimed for PG 1553+113 in the HE band to date.

An extensive multi-wavelength (MWL) observation campaign on PG 1553+113 was carried out from 2012 February to June, focused on the characterization of its SED as well as the variability of the source emission at different frequencies. Observations from VHE γ-rays to radio were performed: VHE band by MAGIC, HE band by *Fermi*-LAT, X-rays by *Swift*-XRT, UV-optical observations by *Swift*-UVOT, IR by REM and radio by Metsähovi and OVRO. In this paper, the study of the flux variability in the VHE, HE and X-ray bands is presented. The study on the VHE spectrum is focused on the April flare state of the source. A detailed study on the long-term MWL campaign will be presented in a forthcoming paper.

The paper is organized as follows: Section 2 describes the MWL data analysis. In Section 3 the results are presented. The light curves from MAGIC, *Fermi*-LAT and *Swift*-XRT are shown in Section 3.1 while a detailed analysis on the observed VHE energy spectrum is presented in Section 3.2. The intrinsic VHE γ-ray spectrum together with a discussion on EBL imprint and redshift constraints can be found in Section 4. The SED observed during the flaring state and the theoretical interpretation is described in Section 5. The conclusions can be found in Section 6.

2 OBSERVATIONS

2.1 VHE γ-ray observations with MAGIC

The VHE γ-ray observations were performed by the MAGIC telescopes. The MAGIC system consists of two 17 m-diameter Imaging Atmospheric Cherenkov Telescopes (IACT) located on the Roque de los Muchachos, Canary Island of La Palma (28°46′ N,17°53′ W), at a height of 2200 m above see level. The system reaches a sensitivity of $(0.76 \pm 0.03)\%$ of the Crab Nebula flux for $E > 290$ GeV in 50 h of observations (Aleksić et al. 2012b).

PG 1553+113 was observed with the MAGIC telescopes from 2012 February to April. The data sample after quality cuts consists of 18.3 hours in the zenith angle range 17° to 34°. The observations were performed in wobble mode (Fomin et al. 1994), with the source located 0.4° from the centre of the field of view. The analysis of the data has been performed using the standard MAGIC analysis chain (Moralejo et al. 2009; Lombardi et al. 2011). The energy threshold of the analysis is approximately 70 GeV.

The source was detected with a high statistical significance (> 70 standard deviations, σ) during the time period 2012 February-April. The emission is compatible with a point-like source at the position of PG 1553+113. The mean γ-rate during the flare period is $4.35 \pm 0.04\,\gamma$/min for $E > 70$ GeV.

2.2 HE γ-rays observations from *Fermi*-LAT

The *Fermi*-LAT is a pair-conversion telescope operating from 20 MeV to > 300 GeV. Further details about the *Fermi*-LAT can be found in Atwood et al. (2009). The LAT data reported in this paper were collected from 2012 February 2 (MJD 55959) to June 10 (MJD 56088). During this period, the *Fermi* observatory operated almost entirely in survey mode. The analysis was performed with the `ScienceTools` software package version v9r32p5. The LAT data were extracted within a 10° region of interest centred at the location of PG 1553+113. Only events belonging to the 'Source' class were used. The time intervals when the rocking angle of the LAT was greater than 52° were rejected. In addition, a cut on the zenith angle (< 100°) was applied to reduce contamination from the Earth limb γ-rays, which are produced by cosmic rays interacting with the upper atmosphere. The spectral analysis was performed with the instrument response functions `P7REP_SOURCE_V15` using an unbinned maximum-likelihood method implemented in the Science tool `gtlike`. Isotropic (iso_source_v05.txt) and Galactic diffuse emission (gll_iem_v05_rev1.fit) components were used to model the background[1] (Ackermann et al. 2012). The normalizations of both components in the background model were allowed to vary freely during the spectral fitting.

We evaluated the significance of the γ-ray signal from the source by means of the maximum-likelihood test statistic TS = 2 (logL_1 - logL_0), where L is the likelihood of the data given the model with (L_1) or without (L_0) a point source at the position of PG 1553+113 (e.g., Mattox et al. 1996). The model of the region of interest used in `gtlike` includes all point sources from the second *Fermi*-LAT catalogue (2FGL; Nolan et al. 2012) as well as from a preliminary third *Fermi*-LAT catalogue from 4 years of survey observations (Ackermann et al., in prep.) that fall within 15° radius around the source. The spectra of these sources were parametrized by power-law functions, except for 2FGL J1504.3.1+1023, 2FGL J1553.5+1255, and 2FGL J1608.5+1029, for which we used a log-parabola as in the 2FGL catalogue. A first maximum-likelihood analysis was performed to remove from the model sources having TS < 10 and/or predicted number of counts based on the fitted model $N_{pred} < 1$. A second maximum-likelihood analysis was performed on the updated source model. In the fitting procedure, the normalization factors and the photon indices of the sources lying within 10° of PG 1553+113 were left as free parameters. For the sources located between 10° and 15°, we kept the normalization and the photon index fixed to the values from the 2FGL catalogue. Integrating over the period from 2012 February 2 to June 10 (MJD 55959-56088) the fit with a power-law model in the 0.1–100 GeV energy range results in a TS = 908, with an integrated average flux of $(5.7 \pm 0.7_{stat}) \times 10^{-8}$ cm^{-2} s^{-1} and a photon index of $\Gamma = 1.59 \pm 0.05_{stat}$ for PG 1553+113. The γ-ray light curve using 10-day time bins is reported in the middle panel of Fig. 1. For each time bin, the spectral shape of PG 1553+113 and all the sources within 10° of it were fixed to the value obtained over the whole period.

The systematic uncertainty in the flux is dominated by the systematic uncertainty in the effective area (Ackermann et al. 2012).

[1] http://fermi.gsfc.nasa.gov/ssc/data/access/lat/BackgroundModels.html

The systematic uncertainty on the effective area amounts to 10% at 100 MeV, decreasing linearly with the logarithm of energy to 5% between 316 MeV and 10 GeV, and increasing linearly with the logarithm of energy up to 10% at 100 GeV[2].

2.3 X-rays and Optical-UV observations from *Swift*

Swift target of opportunity observations (Gehrels et al. 2004) of PG 1553+113 were triggered by an increase of the flux emission observed in the VHE band by the MAGIC telescopes (Cortina et al. 2012a,b). The *Swift* observations were performed in 2012 from February 22 to June 24. Previous observations in 2010 and 2011 have also been used for comparison purposes. The data taken with XRT on board *Swift* were processed with standard procedures (`xrtpipeline v0.12.6`), filtering, and screening criteria by using the `Heasoft`[3] package (v6.12). The data were collected both in photon counting (PC) and windowed timing (WT) mode, and XRT event grades 0–12 and 0–2 for the PC and WT events were selected, respectively (Burrows et al. 2005). Source events in WT mode were extracted from a circular region with a radius of 20 pixels (1 pixel ~ 2.36"), while background events were extracted from a circular region with the same radius away from the source region. Observations in PC mode showed an average count rate of > 0.5 counts s^{-1}, thus requiring pile-up correction. We extracted the source events from an annular region with an inner radius of 5 pixels (estimated by means of the PSF fitting technique) and an outer radius of 30 pixels. We extracted background events within an annular region centered on the source with radii 70 and 120 pixels. Ancillary response files were generated with xrtmkarf, and account for different extraction regions, vignetting and PSF corrections. We used the lastest spectral redistribution matrices in the Calibration database maintained by HEASARC. We fit the spectrum with an absorbed log-parabola (`logpar` in Xspec; e.g. Massaro et al. 2004) using the photoelectric absorption model `tbabs` (Wilms et al. 2000), with a neutral hydrogen column density fixed to its Galactic value (3.65×10^{20} cm^{-2}, Kalberla et al. 2005).

During the *Swift* pointings, the UVOT instrument observed PG 1553+113 in all its optical (v, b and u) and UV ($w1$, $m2$ and $w2$) photometric bands (Poole et al. 2008; Breeveld et al. 2010). We analysed the data using the `uvotsource` task included in the `HEAsoft` package. Source counts were extracted from a circular region of 5″ radius centered on the source, while background counts were derived from a circular region of 10″ radius in the source neighbourhood. Conversion of magnitudes into de-reddened flux densities was obtained by using the E(B-V) value of 0.05205 from Schlegel et al. (1998), the extinction laws by Cardelli et al. (1989) and the magnitude-flux calibrations by Bessell et al. (1998).

2.4 Infrared observations from REM

PG 1553+113 was observed in the IR regime by the REM telescope. The REM (Zerbi et al. 2001; Covino et al. 2004) is a robotic telescope located at the European Southern Observatory (ESO) Cerro La Silla (Chile). It has a Ritchey-Chretien configuration with a 60-cm f/2.2 primary and an overall f/8 focal ratio in a fast moving alt-azimuth mount providing two stable Nasmyth focal stations. At one of the two foci, the telescope simultaneously feeds, by means of a dichroic, two cameras: REMIR for the near-infrared (NIR; Conconi et al. 2004) and REM Optical Slitless Spectrograph (ROSS, Tosti et al. 2004) for the optical. The cameras both have a field of view of 10 arcmin x 10 arcmin and imaging capabilities with the usual NIR (z, J, H and K) and Johnson-Cousins VRI filters. The REM software system (Covino et al. 2004) is able to manage complex observational strategies in a fully autonomous way. All raw optical/NIR frames obtained with the REM telescopes were reduced following standard procedures. Instrumental magnitudes were obtained via aperture photometry and absolute calibration were performed using 2MASS objects in the field. The flux was corrected for Galactic reddening and extinction making use of the Schlafly & Finkbeiner (2011) extinction maps.

2.5 Radio observations from Metsähovi and OVRO

PG 1553+113 was observed by the Metsähovi 13.7-m radio telescope at 37 GHz during the MWL campaign from April to May. The measurements were made with a 1 GHz-band dual beam receiver centered at 36.8 GHz. The observations are ON-ON observations, alternating the source and the sky in each feed horn. A detailed description of the observation and analysis methods can be found in Teräsranta et al (1998). The detection limit (defined as S/N⩾4) of the telescope is of the order of 0.2 Jy under optimal weather conditions. Given the fact that the typical flux density of PG 1553+113 is close to this limit, only half the observations resulted in a detection.

The source is also monitored at 15 GHz using the 40-m telescope of the Owens Valley Radio Observatory (OVRO) as a part of a larger monitoring program where a sample of ~ 1700 sources are observed twice a week (Richards et al. 2011). The telescope is equipped with dual-beamed off-axis optics and a cooled receiver installed at the prime focus. The two sky beams are Dicke switched using the off-source beam as a reference, and the source is alternated between the two beams in an ON-ON fashion to remove atmospheric and ground contamination. Calibration is referenced to 3C 286 for which the flux density of 3.44 Jy at 15 GHz is assumed (Baars et al. 1977). The systematic uncertainty is about 5% in the flux density scale. Details on the observations, calibration and analysis are given in Richards et al. (2011).

3 RESULTS

In this section, a detailed analysis of the γ-ray and X-ray data will be presented. The remaining results are discussed in Section 5.

3.1 Light curve

The light curves at VHE γ-rays, HE γ-rays, and X-rays are shown in Fig. 1. For the VHE and X-rays bands a nightly time-scale is used, while for the HE band we have used a 10-day binning. Clear variability is detected in both VHE and X-ray bands. The hypothesis of a constant flux can be rejected with high confidence level, $P=1.4\times10^{-21}$ ($\chi^2/ndf=143.5/18$) in VHE γ-rays and $P=1.7\times10^{-50}$ ($\chi^2/ndf=302.1/23$) in X-rays. The HE flux is compatible with a constant flux of $F=(5.5\pm0.4)\times10^{-8}$ $cm^{-2}s^{-1}$ for energies 0.1–100 GeV with a fit probability of P=0.6 ($\chi^2/ndf=10.7/12$). Note that the HE light curve is dominated by the emission at E<10 GeV, accounting for the 95% of the photons.

In the VHE band, two states can be differentiated according to the source flux. In 2012 February-March the source flux

[2] http://fermi.gsfc.nasa.gov/ssc/data/analysis/LAT_caveats.html
[3] http://heasarc.nasa.gov/lheasoft/

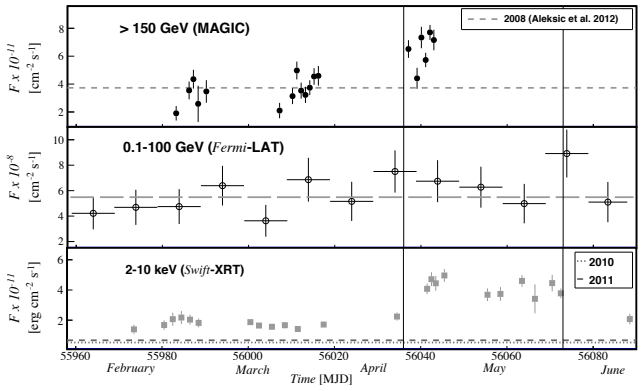

Figure 1. Light curve of PG 1553+113 during the 2012 observation campaign. Upper panel: nightly light curve in VHE γ-rays observed with the MAGIC telescopes for E>150 GeV. For comparison the flux during the high state of the source in 2008 measured by MAGIC (Aleksić et al. 2012a) is shown by the dashed line. Middle panel: *Fermi*-LAT light curve computed with a 10-day binning for energies between 0.1 to 100 GeV; the dashed gray line shows a fit to a constant. Lower panel: flux in the X-ray band in one night bins observed by *Swift*-XRT from 2 to 10 keV is represented in gray squares. For comparison previous measurements from 2010 and 2011 with *Swift*-XRT are plotted as dashed lines. The vertical lines denote flare interval defined in the text.

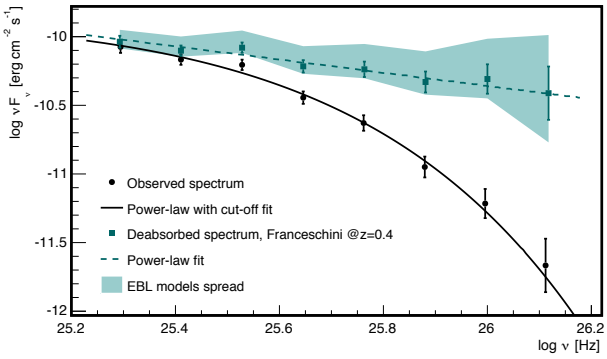

Figure 2. SED of PG 1553+113 as measured by MAGIC during the flare state of 2012 April. The observed SED is shown as black circles, and the black solid line represents the best fit to a power-law with an exponential cut-off. The absorption-corrected spectrum assuming $z = 0.4$ and using the EBL model by Franceschini et al. (2008) is shown by the green squares; the dashed green line is the best-fitting power-law. The green shaded area account for the uncertainties derived by the use of different EBL models.

was at a level comparable with previous high states, as for example, that detected in 2008 (Aleksić et al. 2012a). In 2012 April the source reached the highest flux observed to date, F (E >150 GeV)=(7.7±0.5)×10^{-11} cm^{-2}s^{-1}. According to the flux level, we divided the data into two samples: MJD 55983 to MJD 56016 (high state) and MJD 56037 to MJD 56043 (flare). The probability of a constant fit for both periods independently are low, P=3.2 × 10^{-3} and P=5.1 × 10^{-3}, respectively. During the flare the VHE flux approximately doubled with respect to the high state. This high state was also observed by H.E.S.S. and the results of that study are in preparation.

The X-ray flux observed in 2012 February-March in the 2-10 keV band is compatible with a constant fit (χ^2/ndf=12.7/12, P=0.4), with a mean flux $(1.71 \pm 0.06) \times 10^{-11}$ erg cm^{-2}s^{-1}. In 2012 April-May the source was in a flare state compatible with a constant flux of (4.20 ± 0.14) × 10^{-11} erg cm^{-2}s^{-1} (χ^2/ndf=10.9/9, P=0.3). Later in 2012 June, the source flux decreased to a level compatible with the flux measured during February-March (high state). For comparison, the flux measured in this band from previous observations during 2010 and 2011 was $(0.59 \pm 0.07) \times 10^{-11}$ erg cm^{-2}s^{-1}, $(0.49 \pm 0.07) \times 10^{-11}$ erg cm^{-2}s^{-1} and $(0.64 \pm 0.13) \times 10^{-11}$ erg cm^{-2}s^{-1} measured during MJD 55198, MJD 55232 and MJD 55781, respectively. We can conclude that the X-ray flux doubled during the observation campaign. During the flare state the source reached a level of $\sim 7-10$ times the quiescent flux of the source measured during 2010 and 2011.

Due to the lack of strictly simultaneous observations it is difficult to perform an accurate comparison of the VHE γ and X-ray variability properties. However, the flux evolution in both wavelengths suggests a correlation between the two bands. The SED can, in fact, be properly described in the framework of a one-zone Synchrotron Self Compton (SSC) model, pointing to a common origin of the emission in both energy bands as will be discussed in Section 5,

3.2 VHE observed spectrum

In this paper, only the VHE γ-ray spectrum during the 2012 April flare (MJD 56037-56043) is presented, as mentioned in Section 1. The VHE γ-ray spectra observed by MAGIC in 2012 February-March will be presented in a forthcoming paper.

The VHE SED detected during the flare is represented by black circles in Fig. 2. In Table 1 the differential VHE γ-ray spectrum can be found. It is corrected for instrumental effects by using the Schmelling unfolding algorithm (Albert et al. 2007a).

The observed spectrum shows curvature, and a simple power-law fit can be discarded with a confidence level of 4.7 σ ($P = 2.6 \times 10^{-6}$, $\chi^2/ndf = 36.1/6$). The differential spectrum can be well fit by a power-law with an exponential cut-off with a probability of $P = 0.7$ ($\chi^2/ndf = 2.8/5$) in the energy range from ~70 GeV to 620 GeV:

$$\frac{dF}{dE} = f_0 \cdot \left(\frac{E}{200\,\mathrm{GeV}}\right)^{-\Gamma} \cdot e^{\frac{-E}{E_c}}, \quad (2)$$

with a normalization constant of $f_0 = (3.2 \pm 1.4_{stat} \pm 0.7_{sys}) \times 10^{-9}$cm^{-2}s^{-1}TeV^{-1}, a photon index of $\Gamma = (1.87 \pm 0.37_{stat} \pm 0.15_{sys})$ and $E_c = (110 \pm 20_{stat} \pm 19_{sys})$ GeV. A full description of the systematics uncertainties for the MAGIC data analysis can be found in Aleksić et al. (2012b).

The VHE γ-ray differential energy flux can be also well described by a log-parabola:

$$\frac{dF}{dE} = f_0 \cdot \left(\frac{E}{200\,\mathrm{GeV}}\right)^{-a-b\cdot\log\frac{E}{200\,\mathrm{GeV}}}, \quad (3)$$

where the parameters are given by a flux normalization constant at 200 GeV of $f_0 = (5.12 \pm 0.20_{stat} \pm 1.18_{sys}) \times 10^{-10}$cm^{-2}s^{-1}TeV^{-1}, $a = (3.83 \pm 0.10_{stat})$ and $b = (2.09 \pm 0.41_{stat})$, the systematic uncertainty of the spectral index is estimated to be ±0.15. The goodness of the fit is given by $\chi^2/ndf = 1.8/5$ with a probability $P = 0.9$.

4 THE INTRINSIC VHE γ-RAY SPECTRUM AND THE ROLE OF THE EBL

The VHE γ-ray spectrum is attenuated by the EBL, as described by Eq. 1. The optical depth (τ) depends on the redshift of the VHE

Energy bin [GeV]	Energy [GeV]	Flux [$\mathrm{TeV}^{-1} \times \mathrm{cm}^{-2} \times \mathrm{s}^{-1}$]	Flux uncertainty [$\mathrm{TeV}^{-1} \times \mathrm{cm}^{-2} \times \mathrm{s}^{-1}$]
71.2–93.4	81.5	7.90×10^{-9}	0.83×10^{-9}
93.4–91.1	106.8	3.69×10^{-9}	0.34×10^{-9}
91.1–160.5	139.9	1.99×10^{-9}	0.18×10^{-9}
160.5–210.5	183.2	6.69×10^{-10}	0.73×10^{-10}
210.5–275.9	239.9	2.55×10^{-10}	0.35×10^{-10}
275.9–361.8	314.0	7.10×10^{-11}	1.36×10^{-11}
361.8–474.3	410.6	2.23×10^{-11}	0.62×10^{-11}
474.3–621.9	536.6	4.68×10^{-12}	2.65×10^{-12}

Table 1. VHE differential energy spectra observed during the 2012 flare. First column represents the energy interval, the second the energy centre of each bin, the second the measured flux after unfolding and the last column is the flux uncertainty.

emitter and the energy of the γ-ray. In order to reconstruct the intrinsic spectrum emitted by a blazar, the redshift and the assumption of an EBL model is required. In the case of PG 1553+113, the uncertainty on the redshift prevents a precise estimation of the intrinsic spectrum. We adopt the optical lower limit from Danforth et al. (2010), $z = 0.4$, to study the EBL absorption effect in the observed spectrum, represented in Fig. 2.

The curvature measured in the observed VHE spectrum can have different origins: intrinsic curvature (maximum electron energy is reached), intrinsic self-absorption and/or EBL absorption. The first hypothesis regarding the energy distribution can be discarded and will be discussed in Section 5 in the framework of the SED modeling. The assumption of the robust lower limit given by Danforth et al. (2010) allows us to test the possible contribution of intrinsic effect and EBL attenuation.

Spectral curvature effects in VHE γ-ray spectra have been detected only in a limited number of blazars. However, exponential cut-offs have not been found, especially in nearby blazars, in the energy range ~70-620 GeV (where the cutoff presented here lies). Considering the possible intrinsic absorption due to pair production within the source, two possible scenarios can be envisioned. If the γ-ray emission is produced within the broad line region (BLR) populated with optical-UV photons, a softening of the spectrum around tens of GeV would be expected (e.g., Reimer 2007; Tavecchio & Mazin 2009; Liu & Bai 2006). This is typically the case for flat spectrum radio quasars (FSRQ) showing strong optical emission lines, although usually weak for BL Lacs. In the far dissipation scenario (e.g., Sikora et al. 2008), where the emission of γ-rays is assumed to be outside of BLR, the seed photons would come from the IR torus producing a softening in the spectrum at energies typically higher than 1 TeV. None of these scenarios predict intrinsic absorption between 70 and 620 GeV, especially from BL Lac objects with weak BLR emission.

The high flux of the source reached during the flare state allowed a high precision measurement of its spectrum. In addition, the spectrum extends to lower energies than previous measurements performed during lower flux states (Aleksić et al. 2012a). Despite the quality of the data and the high state of the source, no significant γ-ray emission was detected above 620 GeV, in agreement with previous measurements and with the γ-ray absorption expected by the state-of-the-art EBL models given the redshift limits. According to the present generation of EBL models, the observations during the flare reach an optical depth of $\tau \sim 3$, which corresponds to ~95% photon absorption.

While the observed spectrum shows clear curvature, we find that the spectrum corrected by the EBL effect assuming $z = 0.4$ can be well described by a simple power-law:

$$\frac{dF}{dE} = f_0 \cdot \left(\frac{E}{200\,\mathrm{GeV}}\right)^{-\Gamma}, \quad (4)$$

whose parameters using the Franceschini et al. (2008) EBL model are given by a normalization flux at 200 GeV $f_0 = (9.7 \pm 0.4_{stat} \pm 2.2_{sys}) \times 10^{-10}\mathrm{cm}^{-2}\mathrm{s}^{-1}\mathrm{TeV}^{-1}$ and a photon index of $\Gamma = (2.45 \pm 0.08_{stat} \pm 0.15_{sys})$. The probability of the fit is P=0.9 ($\chi^2/ndf = 2.2/6$). The EBL-corrected spectrum is shown as green squares Fig. 2, while the green shaded area represents the uncertainty when assuming different EBL models (Domínguez et al. 2011; Kneiske & Dole 2010; Franceschini et al. 2008; Gilmore et al. 2012).

We tested for a possible shift of 15% in the energy scale due to the uncertainty in the energy measurement (Aleksić et al. 2012b). This was done by performing an event-wise shift in the data while leaving the Monte Carlo (MC) simulations (which are used to determine the energy of each event) unchanged. This simulates a data/MC mismatch, which could occur for numerous reasons including imperfect atmospheric conditions. Both energy shifted spectra (see Fig. 3), towards lower and higher, are compatible with a power-law fit with $\chi^2/ndf = 6.7/5$ and $\chi^2/ndf = 8.1/6$, respectively. The shift to lower energies results in a steepening of the intrinsic spectrum (EBL-corrected according to Franceschini et al. (2008) model assuming $z = 0.4$) with a spectral index $\Gamma = 3.37 \pm 0.12$, while the shift to higher energies results in an intrinsic VHE γ-ray spectral index of $\Gamma = 2.07 \pm 0.08$.

The fact that the EBL-corrected VHE spectrum, assuming as a redshift the robust optical lower limit (Danforth et al. 2010), is compatible with a simple power-law suggests that the curvature measured in the observed spectrum is very likely due to the interaction of the VHE photons with the EBL.

4.1 Redshift estimates

Different methods to determine an upper limit on the redshift of PG 1553+113 can be applied, taking advantage of the unprecedented high-quality spectrum measured during the 2012 flare.

As a first method, we estimate the redshift of the source using the empirical law calibrated with known distance sources published in Prandini et al. (2010), and later updated using the 1FGL catalog Abdo et al. (2010) in Prandini et al. (2011). More in detail, we find the value z^* at which the de-absorbed VHE slope equals the *Fermi*-LAT slope published in 1FGL catalog (1.66±0.03). Then, considering that for known redshift sources z^* is approximately related to

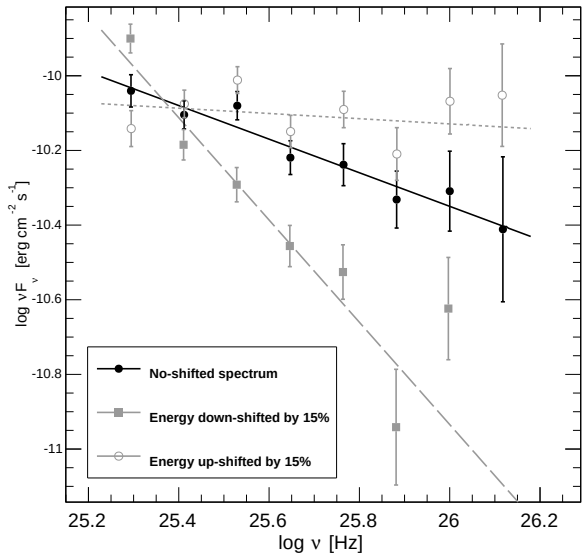

Figure 3. MAGIC spectral energy distribution EBL-corrected with Franceschini et al. (2008) model by assuming $z = 0.4$. The no-shifted spectrum is represented by the black circles. The solid grey squares show the spectrum considering a shift to lower energies by 15%, and the grey open circles represent the spectrum accounting for a shift to higher energies by 15%.

the true redshift by z^*=0.036+1.60·z_{true} (Prandini et al. 2011), it is possible to infer z_{true} by inverting the formula. In this case, we get z^*=0.62±0.04, which leads to the most likely value for the distance of the source of $z_{true} = 0.36 \pm 0.03 \pm 0.05$, where the first error accounts for the statistical uncertainty and includes both MAGIC and *Fermi*/LAT slope errors, while the second refers to the method uncertainty. In the original study from Prandini et al. (2011), systematic errors are not taken into account. We estimate the systematic errors from the combination of the systematics on the slope of *Fermi*/LAT (0.04, Abdo et al. 2009) and MAGIC (0.15) spectra. We find that the systematic error affecting z^* is 0.05, while that on z_{true} is 0.03, respectively. This method to estimate the redshift of PG1553+113 has two additional sources of uncertainties. The first one is that the Fermi GeV and MAGIC TeV spectra are not simultaneous. Given the few hours long observation with MAGIC, the LAT strictly simultaneous spectrum would have very large statistical uncertainties and hence not usable in practice. The second source of uncertainty is that the algorithm relating the spectral slopes and the true redshift of the source was obtained using non-flaring objects, and such relation might differ when the sources flare because that spectral variability is typically much larger at TeV energies than at GeV energies. An estimate of the uncertainty produced by these two effects is not trivial, and is not considered in this study.

The assumption that the slope of the EBL-corrected VHE γ-ray spectrum cannot exceed the slope measured at lower energies by the *Fermi*-LAT can be used to find an upper limit for the redshift. From the value of z^*=0.62±0.04, we find a redshift upper limit of $z < 0.70$ at 95% confidence level.

As a second method, we estimate the upper limit on the redshift by excluding the presence of a pile-up at high energies in the intrinsic VHE γ-ray spectrum. Since an additional spectral component is not expected, a break caused by a hardening of the spectrum can be used as an evidence of over-correction of the spectrum due to an overestimation of the assumed distance. Therefore this method

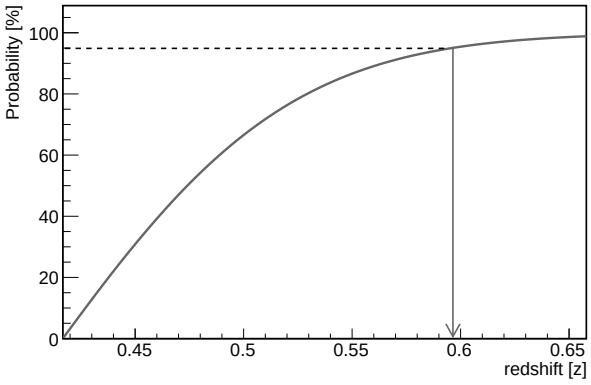

Figure 4. Constraint on the redshift of PG 1553+113 with the likelihood ratio test when comparing the hypothesis of a power-law fit and a positive curved power law (concave) fit for different distances of the source, using the EBL model from Franceschini et al. (2008)

.

can be used to infer an upper limit on the redshift of the source. To find the upper limit, a χ^2 ratio test is performed. This test is used to evaluate the hypothesis of evidence of a break in the intrinsic spectrum, as proposed in Mazin & Goebel (2007). The hypothesis of a simple power-law fitting the EBL-corrected spectrum is compared with that of a curved power-law, which can fit better the possible pile-up. For the PG 1553+113 data used in this work, the resulting probability is plotted in Fig. 4. Above a redshift ~ 0.42 a curved fit with positive curvature, which describes the pile-up, start to describe better the data than a simple power-law. At redshift $z \geqslant 0.60$ a curved fit with positive curvature is preferred to a simple power-law fit at the 95% confidence level. Therefore the assumption that there is no spectral pile-up at high energies gives an upper limit on the source redshift of $z < 0.60$ within a 2-σ confidence interval.

5 SPECTRAL ENERGY DISTRIBUTION

Fig. 5 shows the quasi-simultaneous SED observed during the flare state on 2012 April from γ-rays to radio. The HE differential energy spectrum was derived using *Fermi*-LAT data, which covers the time interval from MJD 56030 to MJD 56088, contemporaneous to the MAGIC observations during the 2012 April flare. The X-ray spectrum shown in Fig. 5 represents the data collected by *Swift*-XRT on MJD 56045. The optical-UV data is the *Swift*-UVOT observation from the same day. The IR flux is estimated from REM telescope observations made on MJD 56046. The radio flux is compatible with a steady emission in both radio bands (37 GHz by (Metsähovi) and 15 GHz by OVRO) and, therefore for the SED shown in Fig. 5, the mean flux from the period MJD 56037-56043 has been used. A full MWL picture can be found in Becerra González et al. (2012).

The SED of PG 1553+113 data during the flare state has been modeled by using a one-zone SSC model (Maraschi & Tavecchio 1993). The emitting region is assumed to be spherical and populated by relativistic electrons. The electron spectrum is assumed to be a smoothed broken power-law as a function of the energy (electron Lorentz factor) between γ_{min} and γ_{max} and break at γ_b:

$$N(\gamma) = K\gamma^{-n1}\left(1 + \frac{\gamma}{\gamma_b}\right)^{n1-n2}, \quad (5)$$

where K is the normalization factor, and n1 and n2 the spectral indices before and after the break. The region is filled with a tangled

magnetic field and moves out of the jet with a given bulk Lorentz factor (Γ). The observable effect of bulk Lorentz factor depends on the viewing angle of the jet, which is taken into account in the Doppler factor (δ) used for the SED modeling. According to the SSC model, the electrons emit synchrotron radiation due to their interaction with the magnetic field creating a low energy photon field, which can in turn interact with the same population of electrons via inverse Compton, producing the high energy emission.

The parameters used for the modeling as well as those of SSC models fitting previous observations of the source in different states, for comparison purpose, can be found in Table 2. The main difference with previous states of the source is that during the strong flare in 2012 the inverse Compton (IC) energy peak moved to higher energies and that more energetic particles were involved. The magnetic field is found to have a lower value with respect to previous high states ('maximum' in Table 2). The emitting region size is larger than in previous cases. However, as given by the causality relation $R < (c \cdot t \cdot \delta)/(1+z)$, the allowed flux variability time-scale is $\sim$ 19 hours (assuming z=0.4), which is compatible with the variability detected in the source as shown in Fig. 1. With respect to the energetics, the electron and proton luminosities are higher while the magnetic field luminosity is lower than previous high states. This could point to different origins of the high states of the source.

As shown in Fig. 5, the increasing part of both SED bumps shows less variability when compared with the decreasing part. This fact is also in agreement with the light curve discussion on Section 3.1: while X-rays and VHE γ-rays show an increase of the flux in 2012, the emission in the HE band is compatible with a constant flux. The high variability found in X-rays and VHE γ-rays suggests that the flaring activity of this source is driven by the most energetic electrons. Moreover, as discussed previously, the SSC model gives a lower magnetic field, which implies a longer synchrotron cooling time-scale. This is in agreement with the displacement of the synchrotron peak to higher frequencies, as well as with the higher variability in the high energy component of both peaks.

As shown in Fig. 5, the IC peak of the SED is close to the VHE band. Therefore, curvature would be expected in the intrinsic VHE SED due to the distribution of the relativistic electrons, within the one-zone SSC framework (as mentioned in Sec. 4). To test if our observations are sensitive enough to detect the expected intrinsic SED curvature, we simulate the MAGIC response assuming the intrinsic emission given by the best-fitting SSC model to the MWL data shown in Fig. 5. We simulate intrinsic VHE SEDs assuming the same frequency sampling and relative errors as in the observed VHE spectral points (only statistical uncertainties have been taken into account). The result of ten thousand realizations are shown in Fig. 6, and are represented by the gray shaded area. Despite the simulated SEDs having, by construction, an evident curvature, 99.2% of the realizations are well described by a simple power-law at 3-σ confidence level. The mean probability of a simple power-law fit is P = 0.44±0.28 with a mean spectral index of 0.38 ± 0.10. We therefore conclude that the sensitivity of our VHE measurements do not allow the detection of an intrinsic curvature in the SSC framework and the EBL model from Franceschini et al. (2008).

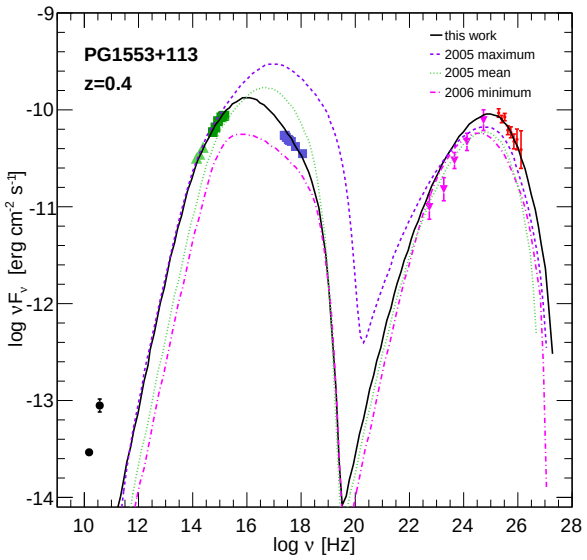

Figure 5. Spectral energy distribution of PG 1553+113 during the 2012 April flare state modeled with the one-zone SSC model of Maraschi & Tavecchio (1993). From high to low energies: the EBL-corrected MAGIC spectra using Franceschini et al. (2008) assuming z=0.4 (red dots, see text), the *Fermi*-LAT data from MJD 55959-56088 (pink triangles), *Swift*-XRT (purple squares) and *Swift*-UVOT (green squares) data from MJD 56045 (good representation of the X-ray and optical-UV state during the VHE flare), IR data from REM (green triangles) from MJD 56047 and mean radio observation in the period MJD 55959-56088 from Metsähovi (black square) and OVRO (black circle). For comparison, the SSC models for previous source states (Aleksić et al. 2012a) have been plotted in colored dashed lines.

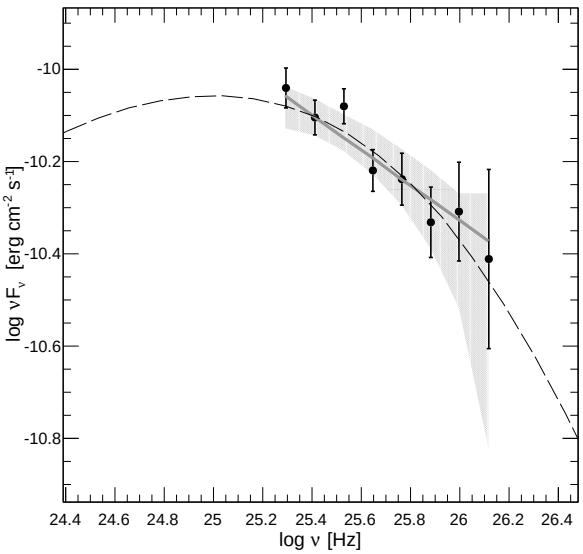

Figure 6. PG 1553+113 VHE SED. The gray shaded area represents the simulated MAGIC response assuming the intrinsic emission given by the best-fitting SSC model to the MWL data shown in Fig. 5. The gray solid line represents the mean power-law fit of the ten thousand realizations of the toy-MC. The black circles denote the PG 1553+113 VHE spectrum EBL-corrected with Franceschini et al. (2008) model assuming z=0.4. The dashed black line represent the best-fitting SSC model from Fig. 5.

6 CONCLUSIONS

In this paper we have presented the highest flux state ever detected from the blazar PG 1553+113 in VHE γ-rays. The flare was de-

Model	$\gamma_{\rm min}$ [10^3]	$\gamma_{\rm b}$ [10^4]	$\gamma_{\rm max}$ [10^5]	n_1	n_2	B [G]	K [cm^{-3}]	R [10^{16}cm]	δ	L$_{kin(e)}$ [10^{45} erg s^{-1}]	L$_{kin(p)}$ [10^{44} erg s^{-1}]	L$_B$ [10^{43} erg s^{-1}]	log10($\nu_{\rm syn}$)
This work	3.7	3.6	8.0	1.60	3.83	0.045	19.5	6.0	40	2.18	1.49	5.83	16.1
Maximum[a]	1.0	3.0	5.2	2.00	3.75	0.800	3.8×10^3	1.0	35	0.52	0.6	39.2	17.0
Minimum[a]	5.0	1.3	4.1	2.00	3.55	0.200	25.0×10^3	1.0	35	0.52	0.6	2.5	15.9
Mean[a]	1.5	3.2	2.2	2.00	4.00	0.500	5.4×10^3	1.0	35	0.52	0.6	15.3	16.7

Table 2. One-zone SSC model parameters of the SED fit during the flare state on 2012. The models marked as [a] correspond to previous activity states of the source (see Aleksić et al. 2012a) and are shown for comparison. The following quantities are reported: the minimum, break, and maximum Lorentz factors and the low and high energy slope of the electron energy distribution, the magnetic field intensity, the electron density, the radius of the emitting region and the Doppler factor, the kinetic energy of the electrons, (cold) protons (assuming one proton per emitting electron), and magnetic field, and the frequency of the synchrotron peak.

tected at VHE by the MAGIC telescopes and monitored in HE γ-rays by *Fermi*-LAT, in X-rays by *Swift*-XRT, in optical-UV by *Swift*-UVOT, in infrared by REM, and in radio by Metsähovi and OVRO. While clear variability has been found in both bands, the VHE and X-rays, HE γ-ray flux is compatible with constant emission.

For the first time spectral curvature compatible with an exponential cut-off has been measured in the energy range from 70 to 620 GeV from a distant blazar ($z \geqslant 0.4$). This curvature most likely originates from EBL absorption if the distance to the source is between the redshift limits measured by Danforth et al. (2010) ($0.4 < z < 0.58$). If the real redshift of this source is higher than these limits, the effect would be a hardening of the spectrum or the (unexpected) presence of a pile-up in the intrinsic spectrum, which would denote that either the EBL models predict an overestimated EBL level or there is a second emission component at high energies.

A redshift upper limit of $z < 0.60$ at 95% C.L. has been derived using the χ^2 ratio test (Mazin & Goebel 2007). The use of a maximum hardness criterion has given a similar result ($z < 0.62$). The most likely value for the redshift of the source has been estimated as $z = 0.36 \pm 0.03_{stat} \pm 0.03_{sys} \pm 0.05_{method}$ using the prescription reported in Prandini et al. (2010).We conclude, that the results of our different methods to estimate the redshift of the source are consistently close to the lower limit of z >0.4 set by Danforth et al. (2010).

A quasi-simultaneous SED has been compiled for the flare episode in 2012 April. It can be well modeled by a one-zone SSC model. The comparison with previous flux states of the source reveals that the higher frequency part of each SED bump shows higher variability than the lower frequency part. This fact points to a scenario where the most energetic electrons play a leading role during the flare episodes of the source.

A detailed study of the MWL behaviour and evolution of the SED will be published in a forthcoming paper.

ACKNOWLEDGEMENTS

We would like to thank the Instituto de Astrofísica de Canarias for the excellent working conditions at the Observatorio del Roque de los Muchachos in La Palma. The support of the German BMBF and MPG, the Italian INFN, the Swiss National Fund SNF, and the ERDF funds under the Spanish MINECO is gratefully acknowledged. This work was also supported by the CPAN CSD2007-00042 and MultiDark CSD2009-00064 projects of the Spanish Consolider-Ingenio 2010 programme, by grant 127740 of the Academy of Finland, by the Croatian Science Foundation (HrZZ) Project 09/176, by the DFG Collaborative Research Centers SFB823/C4 and SFB876/C3, and by the Polish MNiSzW grant 745/N-HESS-MAGIC/2010/0. Part of this work has been possible with the support of the Cluster of Excellence: "Connecting Particles with the Cosmos", part of the Landesexzellenzinitiative Hamburg. The authors thank to S. Buson, J. Finke, J. Perkins and A. Neronov for their comments and contributions. JBG would like to thanks to M. Raue for useful discussions.

The *Fermi* LAT Collaboration acknowledges generous ongoing support from a number of agencies and institutes that have supported both the development and the operation of the LAT as well as scientific data analysis. These include the National Aeronautics and Space Administration and the Department of Energy in the United States, the Commissariat à l'Energie Atomique and the Centre National de la Recherche Scientifique / Institut National de Physique Nucléaire et de Physique des Particules in France, the Agenzia Spaziale Italiana and the Istituto Nazionale di Fisica Nucleare in Italy, the Ministry of Education, Culture, Sports, Science and Technology (MEXT), High Energy Accelerator Research Organization (KEK) and Japan Aerospace Exploration Agency (JAXA) in Japan, and the K. A. Wallenberg Foundation, the Swedish Research Council and the Swedish National Space Board in Sweden. Additional support for science analysis during the operations phase is gratefully acknowledged from the Istituto Nazionale di Astrofisica in Italy and the Centre National d'Études Spatiales in France.

We thank the *Swift* team duty scientists and science planners for making these observations possible;

The OVRO 40-m monitoring program is supported in part by NASA grants NNX08AW31G and NNX11A043G, and NSF grants AST-0808050 and AST-1109911.

The Metsähovi team acknowledges support from the Academy of Finland to our observing projects (numbers 212656, 210338, 121148, and others).

REFERENCES

Abdo, A. A., et al. 2009, ApJ, 707, 1310
Abdo A. A. et al., 2010, ApJ, 708, 1310
Abdo, A. A., et al. 2010b, ApJS, 188, 405
Aharonian F. et al. (H.E.S.S. Coll.), 2006a, A&A, 448, L19
Aharonian F. et al., 2006b, Nature, 440, 1018
Albert J. et al. (MAGIC Coll.), 2007, ApJ Letters, 654, L119

Ackermann M. et al., 2012, ApJS 203, 4
Aleksić J. et al. (MAGIC Coll.), 2012a, ApJ, 748, 46
Aleksić J. et al. (MAGIC Coll.), 2012b, APh, 35, 435
Atwood W. B. et al., 2009, ApJ, 697, 1071
Baars J. W. M. et al., 1977, A&A, 61, 99
Beasley A. J. et al., 2002, ApJS, 141, 13
Becerra González, J. et al. (MAGIC Coll.), 2012, in AIP Proc. Gamma2012 (Heidelberg)
Bessell M. S., Castelli F., Plez B., 1998, A&A, 333, 231
Breeveld A. A. et al., 2010, MNRAS, 406, 1687
Burrows D. N. et al., 2005, SSRv, 120,165
Cardelli J. A., Clayton G. C., Mathis J. S., 1989, ApJ, 345, 245
Conconi P. et al., 2004, in Moorwood A. F. M., Masanori I., eds, Proc. SPIE, Conf. Ser. Vol. 5492, Ground-based Instrumentation for Astronomy. SPIE, Bellingham, p. 1602
Cortina J. et al. (MAGIC Coll.), 2012a, Astronomer's Telegram 3977
Cortina J. et al. (MAGIC Coll.), 2012b, Astronomer's Telegram 4069
Covino S. et al., 2004, in Moorwood A. F. M., Masanori I., eds, Proc. SPIE, Conf. Ser. Vol. 5492, Ground-based Instrumentation for Astronomy. SPIE, Bellingham, p. 1613
Danforth C.W., Keeney A. B., Stocke J.T., Micheal Shull J., Yao J., 2010, ApJ, 720, 976
Domínguez A. et al., 2011, MNRAS, 410, 2556
Domínguez A. et al., 2013, ApJ, 770, 77, 15 pp.
Finke J. D. et al., 2010, ApJ, 712, 1, 238-249 pp.
Franceschini A., Rodighiero G., Vaccari M., 2008, A&A, 487, 837
Fomin V. P. et al., 1994, ApJ, 2, 137
Gehrels N. et al., 2004, ApJ, 611, 1005
Gilmore R. et al., 2012, MNRAS, 422, 3189-3207
Green R.F., Schimdt M., Liebert J., 1986, ApJS, 61, 305
Hauser M. G., Dwek E., 2001, ARA&A, 39, 249
Kalberla P. M. W. et al., 2005, A&A, 440, 775
Kneiske T. M., Dole H., 2010, A&A, 515, 19
Li T.-P., Ma Y.-Q., 1983, ApJ, 272, 317
Liu H. T., Bai J. M., 2006, ApJ, 653, 1089
Lombardi S. et al., 2011, in Proc. 32nd ICRC (Beijing) (arXiv:1109.6195)
Mankuzhiyil N. et al., 2010, ApJ 715 L16
Maraschi L., Tavecchio F., 2003, ApJ, 593, 667
Massaro E. et al., 2004, A&A, 413, 489
Mattox J. R. et al., 1996, ApJ, 461, 396
Mazin D., Goebel F., 2007, ApJ, 655, L13
Miller H. R., Green R. F., 1983, BAAS, 15, 957
Miller H. R. et al., 1988, ESA Special Publication, 281, 303
Moralejo A. et al., 2009, in Proc. 31st ICRC (Lódź) (arXiv:0907.0943)
Nolan P. L. et al., 2012, Ap.J.Supp., 199, 31
Prandini E. et al., 2010, MNRAS, 405, L76
Prandini, E. et al., 2011, in Proceedings CRF2010 (preprint: arXiv:1101.5005)
Poole T. S. et al., 2008, MNRAS, 383, 627
Reimer A., 2007, ApJ, 665, 1023
Richards J. L. et al., 2011, ApJS, 194, 29
Sbarufatti B., Treves A., Falomo R., 2005, ApJ, 635, 173
Sbarufatti B. et al., 2006, AJ, 132, 1
Schlafly E. F., Finkbeiner D. P., 2011, ApJ, 737, 103
Schlegel D. J., Finkbeiner D. P., Davis M., 1998, ApJ, 500, 525
Scully S. T., Malkan M. A., Stecker F. W., 2014, ApJ, 784, 138
Shaw M. S. et al., 2013, ApJ, 764 135
Sikora M., Moderski R., Madejski G. M., 2008, ApJ, 675, 71
Stecker F. W., DeJager O. C., Salamon M. H., 1992, ApJ, 390, L49
Stecker F., Malkan M., Scully S., 2006, ApJ, 648, 774
Teräsranta H. et al., 1998, A&AS, 132, 305
Tavecchio F., Mazin D., 2009, MNRAS, 392, L40
Tosti G. et al., 2004, in Moorwood A. F. M., Masanori I., eds, Proc. SPIE Conf. Ser. Vol. 5492, Ground-based Instrumentation for Astronomy, SPIE, Bellingham, p. 689
Wilms J. et al., 2000, ApJ, 542, 914
Zerbi R. M. et al., 2001, Astron. Nachr., 322, 275

[1] IFAE, Campus UAB, E-08193 Bellaterra, Spain
[2] Università di Udine, and INFN Trieste, I-33100 Udine, Italy
[3] INAF National Institute for Astrophysics, I-00136 Rome, Italy
[4] Università di Siena, and INFN Pisa, I-53100 Siena, Italy
[5] Croatian MAGIC Consortium, Rudjer Boskovic Institute, University of Rijeka and University of Split, HR-10000 Zagreb, Croatia
[6] Max-Planck-Institut für Physik, D-80805 München, Germany
[7] Universidad Complutense, E-28040 Madrid, Spain
[8] Inst. de Astrofísica de Canarias, E-38200 La Laguna, Tenerife, Spain
[9] University of Łódź, PL-90236 Lodz, Poland
[10] Deutsches Elektronen-Synchrotron (DESY), D-15738 Zeuthen, Germany
[11] ETH Zurich, CH-8093 Zurich, Switzerland
[12] Universität Würzburg, D-97074 Würzburg, Germany
[13] Centro de Investigaciones Energéticas, Medioambientales y Tecnológicas, E-28040 Madrid, Spain
[14] Institute of Space Sciences, E-08193 Barcelona, Spain
[15] Università di Padova and INFN, I-35131 Padova, Italy
[16] Technische Universität Dortmund, D-44221 Dortmund, Germany
[17] Unitat de Física de les Radiacions, Departament de Física, and CERES-IEEC, Universitat Autònoma de Barcelona, E-08193 Bellaterra, Spain
[18] Universitat de Barcelona, ICC, IEEC-UB, E-08028 Barcelona, Spain
[19] Japanese MAGIC Consortium, Division of Physics and Astronomy, Kyoto University, Japan
[20] Finnish MAGIC Consortium, Tuorla Observatory, University of Turku and Department of Physics, University of Oulu, Finland
[21] Inst. for Nucl. Research and Nucl. Energy, BG-1784 Sofia, Bulgaria
[22] Università di Pisa, and INFN Pisa, I-56126 Pisa, Italy
[23] ICREA and Institute of Space Sciences, E-08193 Barcelona, Spain
[24] Università dell'Insubria and INFN Milano Bicocca, Como, I-22100 Como, Italy
[25] now at: NASA Goddard Space Flight Center, Greenbelt, MD 20771, USA and Department of Physics and Department of Astronomy, University of Maryland, College Park, MD 20742, USA
[26] now at Ecole polytechnique fédérale de Lausanne (EPFL), Lausanne, Switzerland
[27] now at Institut für Astro- und Teilchenphysik, Leopold-Franzens- Universität Innsbruck, A-6020 Innsbruck, Austria
[28] now at Finnish Centre for Astronomy with ESO (FINCA), Turku, Finland
[29] also at INAF-Trieste
[30] also at ISDC - Science Data Center for Astrophysics, 1290,

Versoix (Geneva)
[31] INAF-IRA, I-40129 Bologna, Italy
[32] Aalto University Metsähovi Radio Observatory, Metsähovintie 114, 02540, Kylmälä, Finland
[33] Aalto University Department of Radio Science and Engineering, Espoo, Finland
[34] Cahill Center for Astronomy & Astrophysics, Caltech, 1200 E. California Blvd, Pasadena, CA, 91125, U.S.A.
[35] Department of Physics, Purdue University, 525 Northwestern Ave, West Lafayette, IN 47907, USA